TECHNICAL RESEARCH REPORT

A Robust Control Framework for Smart Actuators

by Xiaobo Tan and John S. Baras

CDCSS TR 2002-5
(ISR TR 2002-39)

The Center for Dynamics and Control of Smart Structures (CDCSS) is a joint Harvard University, Boston University, University of Maryland center, supported by the Army Research Office under the ODDR&E MURI97 Program Grant No. DAAG55-97-1-0114 (through Harvard University). This document is a technical report in the CDCSS series originating at the University of Maryland.

Web site http://www.isr.umd.edu/CDCSS/cdcss.html

ACC03-IEEE0650

A Robust Control Framework for Smart Actuators*

Xiaobo Tan and John S. Baras
Institute for Systems Research and
Department of Electrical and Computer Engineering
University of Maryland, College Park, MD 20742 USA
{xbtan, baras}@isr.umd.edu

Abstract

Hysteresis in smart actuators presents a challenge in control of these actuators. A fundamental idea to cope with hysteresis is inverse compensation. But due to the open loop nature of inverse compensation, its performance is susceptible to model uncertainties and to errors introduced by inverse schemes. In this paper we develop a robust control framework for smart actuators by combining inverse control with the l_1 robust control theory, where the inversion error is modeled as an exogenous disturbance with a magnitude bound quantifiable in terms of parameter uncertainties and inversion schemes. Through the example of controlling a magnetostrictive actuator, we present a systematic controller design method which guarantees robust stability and robust trajectory tracking while taking actuator saturation into account. Simulation and experimental results are provided.

1 Introduction

Smart materials, such as magnetostrictives, piezoelectrics, shape memory alloys (SMAs), and magnetorheological (MR) fluids, all display certain coupling phenomena between applied electromagnetic/thermal fields and their mechanical/rheological properties. Smart actuators and sensors made of these materials have been receiving tremendous interest due to their broad applications in areas of aerospace, manufacturing, defense, and civil infrastructure systems, to name a few. The hysteretic behavior widely existing in smart materials, however, makes the effective use of these actuators and sensors quite challenging.

*This research was supported by the Army Research Office under the ODDR&E MURI97 Program Grant No. DAAG55-97-1-0114 to the Center for Dynamics and Control of Smart Structures (through Harvard University).

Models for smart actuators that capture both hysteresis and dynamic behaviour have a cascaded structure as shown in Figure 1(a) [1], where W is a hysteretic operator (with possibly some other nonlinearities) and $\hat{G}_a(\lambda)$ is a linear system. In this paper we consider the discrete-time setting in the interest of digital control, and $\hat{G}(\lambda)$ denotes the λ-transform of a linear time-invariant (LTI) system G. We recall that the λ-transform $\hat{G}(\lambda)$ is just the usual z-transform of G with $\lambda = z^{-1}$ [2].

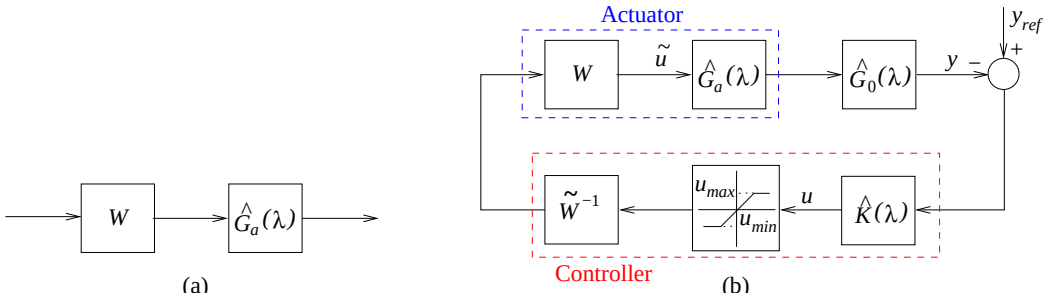

Figure 1: (a) The model structure for smart actuators; (b) The closed-loop system incorporating inverse compensation.

In Figure 1(b), $\hat{G}_0(\lambda)$ denotes the plant to be controlled by the actuator. A basic approach to cope with the hysteresis is to design an (approximate) right inverse operator $\tilde{W}^{-1}$ for W, then $\tilde{u} \approx u$ and the controller design problem is reduced to designing a linear controller $\hat{K}(\lambda)$ for the composite linear system $\hat{G}_0(\lambda) \circ \hat{G}_a(\lambda)$. The idea of inverse compensation can be found in, e.g., [3, 4, 5, 6, 7].

The most popular hysteresis model used in control of smart actuators has been the Preisach operator [3, 8, 9, 7]. The Preisach operator provides a means of developing phenomenological models that are capable of producing behaviors similar to those of physical systems. For a detailed treatment of the Preisach operator, we refer to [10, 11, 12].

Due to the open loop nature of inverse compensation, its performance is susceptible to model uncertainties and to errors introduced by inversion schemes. To combat this problem, adaptive inverse control schemes were proposed for a class of hysteresis nonlinearities with parameterizable inverses [4, 13]. For the Preisach operator-based hysteresis models, however, their inverses are not parameterizable in general. In this paper we develop a robust control framework for smart actuators by combining inverse control with the l_1 control techniques [2]. The inversion error is modeled as an exogenous disturbance with a magnitude bound quantifiable in terms of parameter uncertainties and inversion schemes. The design requirements for the controller $\hat{K}(\lambda)$ can be roughly stated as: in the presence of the inversion error and the uncertainties in $\hat{G}_a$ and $\hat{G}_0$, for all desired trajectories in a certain class, a) the closed-loop system

is stable, b) the tracking error is minimized, and c) the output of $\hat{K}$ does not exceed the saturation limits. We take the saturation constraint (a common nonlinearity for actuators) into account in the design of $\hat{K}$ to ensure that the overall system operates in the linear region and thus predictions based on the linear design are credible. The controller design method will be illustrated through the example of robust trajectory tracking of a magnetostrictive actuator.

The remainder of the paper is organized as follows. In Section 2 we introduce the Preisach operator and an identification scheme for the Preisach operator. In Section 3 we describe the model for a magnetostrictive actuator. We discuss quantification of bounds on inversion errors in Section 4. We then formulate and solve the robust control problem in Section 5. Simulation and experimental results are provided in Section 6. Finally we conclude in Section 7.

2 The Preisach Model

For a pair of thresholds (β, α) with $\beta \leq \alpha$, consider a simple hysteretic element $\hat{\gamma}_{\beta,\alpha}[\cdot,\cdot]$, as illustrated in Figure 2. For $u \in C([0,T])$ and an initial configuration $\zeta \in \{-1, 1\}$, the function $v = \hat{\gamma}_{\beta,\alpha}[u,\zeta] : [0,T] \to \{-1,1\}$ is defined as follows [11]:

$$v(0) \stackrel{\triangle}{=} \begin{cases} -1 & \text{if } u(0) \leq \beta \\ \zeta & \text{if } \beta < u(0) < \alpha \\ 1 & \text{if } u(0) \geq \alpha \end{cases},$$

and for $t \in (0,T]$, setting $X_t \stackrel{\triangle}{=} \{\tau \in (0,t] : u(\tau) = \beta \text{ or } \alpha\}$,

$$v(t) \stackrel{\triangle}{=} \begin{cases} v(0) & \text{if } X_t = \emptyset \\ -1 & \text{if } X_t \neq \emptyset \text{ and } u(\max X_t) = \beta \\ 1 & \text{if } X_t \neq \emptyset \text{ and } u(\max X_t) = \alpha \end{cases}.$$

This operator is sometimes referred to as an *elementary Preisach hysteron* (we will call it a *hysteron* in this paper), since it is a building block for the Preisach operator.

The Preisach operator is a weighted superposition of all possible hysterons. Define $\mathcal{P}_0 \stackrel{\triangle}{=} \{(\beta,\alpha) \in \mathbb{R}^2 : \beta \leq \alpha\}$. $\mathcal{P}_0$ is called the *Preisach plane*, and each $(\beta,\alpha) \in \mathcal{P}_0$ is identified with the hysteron $\hat{\gamma}_{\beta,\alpha}$. For $u \in C([0,T])$ and a Borel measurable initial configuration ζ_0 of all hysterons: $\zeta_0 : \mathcal{P}_0 \to \{-1,1\}$, the

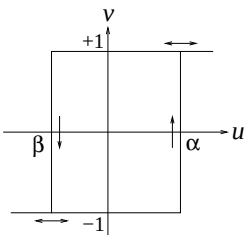

Figure 2: The elementary Preisach hysteron.

output of the Preisach operator Γ is defined as [11]:

$$y(t) = \Gamma[u, \zeta_0](t) = \int_{\mathcal{P}_0} \hat{\gamma}_{\beta,\alpha}[u, \zeta_0(\beta, \alpha)](t) d\nu(\beta, \alpha), \tag{1}$$

where ν is a finite, signed Borel measure on $\mathcal{P}_0$, called the *Preisach measure*.

We call the Preisach measure ν *nonsingular* if $|\nu|$ is absolutely continuous with respect to the two-dimensional Lebesgue measure, and *singular* otherwise. By the Radon-Nikodym theorem [14], if ν is nonsingular, there exists a Borel measurable function μ, such that

$$\Gamma[u, \zeta_0](t) = \int \int_{\mathcal{P}_0} \mu(\beta, \alpha) \hat{\gamma}_{\beta,\alpha}[u, \zeta_0(\beta, \alpha)](t) d\beta d\alpha. \tag{2}$$

The weighting function μ is often referred to as the *Preisach function* [10] or the *density function* [12].

To simplify the discussion, throughout the paper we assume that μ has a compact support, i.e., $\mu(\beta, \alpha) = 0$ if $\beta < \beta_0$ or $\alpha > \alpha_0$ for some β_0, α_0, and without loss of generality, we let $\alpha_0 = -\beta_0 =: r_0 > 0$. Then it suffices to consider the finite triangular area $\mathcal{P} \stackrel{\triangle}{=} \{(\beta, \alpha) \in \mathbb{R}^2 | \alpha \geq \beta, \beta \geq -r_0, \alpha \leq r_0\}$.

At time t, $\mathcal{P}$ can be divided into two regions: $\mathcal{P}_{\pm}(t) \stackrel{\triangle}{=} \{(\beta, \alpha) \in \mathcal{P} |$ output of $\hat{\gamma}_{\beta,\alpha}$ at t is $\pm 1\}$. In most cases of interest, each of $\mathcal{P}_-$ and $\mathcal{P}_+$ is a connected set [10], and the output of Γ is determined by the boundary between $\mathcal{P}_-$ and $\mathcal{P}_+$ if the Preisach measure is nonsingular. The boundary is also called the *memory curve*. The memory curve has a staircase structure and its intersection with the line $\alpha = \beta$ gives the current input value. The memory curve ψ_0 at $t = 0$ is called the *initial memory curve* and it represents the initial condition of the Preisach operator.

If the Preisach measure is nonsingular, we can identify a configuration of hysterons ζ_ψ with a memory curve ψ in the following way: $\zeta_\psi(\beta, \alpha) = 1\,(-1, \text{resp.})$ if (β, α) is below (above, resp.) the graph of ψ. Note that it does not matter whether ζ_ψ takes 1 or -1 on the graph of ψ. In the sequel we will put the initial memory curve ψ_0 as the second argument of Γ, where $\Gamma[\cdot, \psi_0] \stackrel{\triangle}{=} \Gamma[\cdot, \zeta_{\psi_0}]$.

A constrained least squares scheme was proposed to identify the Preisach measure in [7]. In the scheme, the input is discretized into $L+1$ levels for some $L > 0$ and that leads to a discretized Preisach operator (Figure 3), i.e., a weighted sum of finitely many hysterons. What is identified in [7], is a collection of weighting masses sitting at centers of cells in the discretization grid (see the dark dots in Figure 3), which forms a singular Preisach measure. We can then obtain a nonsingular approximation ν_p to the true Preisach measure ν by assuming each identified mass is distributed uniformly over the corresponding cell. Note that the density μ_p corresponding to ν_p is piecewise uniform.

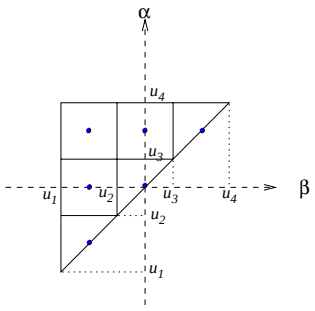

Figure 3: Discretization of the Preisach plane ($L = 3$).

3 The Model for Magnetostrictive Actuators

Magnetostriction is the phenomenon of strong coupling between magnetic properties and mechanical properties of some ferromagnetic materials (e.g., Terfenol-D). Figure 4 shows a sectional view of a Terfenol-D actuator. By varying the current in the coil, we vary the magnetic field in the Terfenol-D rod and thus control the displacement of the rod head.

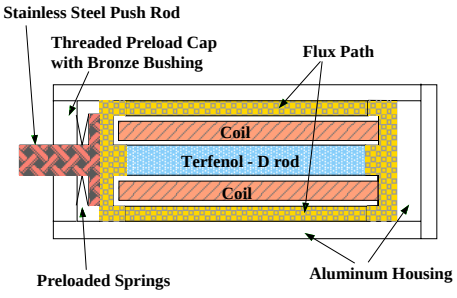

Figure 4: Sectional view of a Terfenol-D actuator [15](Original source: Etrema Products, Inc.).

When the input frequency is low (typically below 5 Hz), the magnetostrictive hysteresis is rate-independent: roughly speaking, the shape of the hysteresis loop is independent of the input frequency,

and a model for the actuator is [7]:

$$\begin{cases} H(t) = c_0 I(t) \\ M(t) = \Gamma[H(\cdot), \psi_0](t) \\ y(t) = c_M M^2(t) \end{cases}, \tag{3}$$

where I is the input current, y is the displacement of the actuator head, M and H are the bulk magnetization and the magnetic field (assumed uniform) along the rod direction, respectively, Γ is the Preisach operator, and c_0 and c_M are positive constants.

When the input frequency gets high, the magnetostrictive hysteresis is rate-dependent. Venkataraman and Krishnaprasad proposed a bulk magnetostrictive hysteresis model for the thin rod actuator based on energy balancing principles [16, 15]. The model has a cascaded structure as shown in Figure 5. Note the resemblance of Figure 5 with Figure 1(a). $\bar{W}$ takes care of the M - H hysteresis and the eddy current losses, and the magnetoelastic dynamics of the rod is lumped into a second order linear system $G(s)$. $G(s)$ has a state space representation [16, 15](after some manipulations):

$$\ddot{y}(t) + 2\xi\omega_0\dot{y}(t) + \omega_0^2 y(t) = \omega_0^2 c_M M^2(t), \tag{4}$$

where ω_0 and ξ are positive constants.

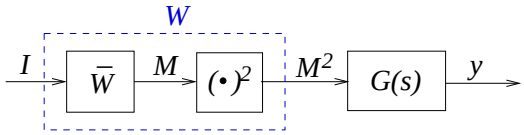

Figure 5: Model structure of a magnetostrictive actuator.

By replacing the switching ODE model in [16, 15] with a Preisach operator Γ for the M - H hysteresis, we have proposed a new dynamic model [17, 18] for the $\bar{W}$ block:

$$\begin{cases} \dot{H}(t) + \dot{M}(t) = c_1(I(t) - \frac{H(t)}{c_0}) \\ M(t) = \Gamma[H(\cdot), \psi_0](t) \end{cases}, \tag{5}$$

where c_1 is a positive constant.

Note if we set derivatives in (4) and (5) to zero, the dynamic model degenerates to the rate-independent hysteresis model (3).

Remark 3.1 *A variety of smart actuators have been modeled by essentially the Preisach operator alone as (3), e.g., see [3, 9]. On the other hand, the rate-dependent model (4) and (5) captures important*

dynamic effects in the frequency region of practical interest. We choose the magnetostrictive actuator as the example, because this allows us to cover both the rate-independent case and the rate-dependent case.

4 Quantification of the Inversion Error

Recall Figure 1(b). There are two possible ways to model the inversion $e_u = \tilde{u} - u$. The first one is to model it as the output of some uncertainty block Δ, and the other one is to simply model it as an exogenous disturbance v. For the Preisach operator-based models, e_u is independent of u and it is possible that $e_u \neq 0$ for $u = 0$. Therefore there exists no stable Δ such that $e_u = \Delta u$, and we will treat $e_u = v$ as an external noise.

The inversion error for the Preisach operator is bounded in magnitude instead of in energy. Hence a natural choice for the signal spaces is l_∞ and not l_2. Also it is more appropriate to use l_∞ for the desired trajectory and the tracking error. Another advantage of using l_∞ for signals is that the actuator saturation constraint can be easily handled in the corresponding l_1 robust control theory, while it's very hard to be formulated in the $\mathcal{H}_\infty$ control theory.

We now quantify the error bounds in inversion of the Preisach operator and the dynamic model (5). Here we are concerned with $e_M = \tilde{M} - M$, where $\tilde{M}$ and M denote the trajectories of achieved magnetization and desired magnetization, respectively. The bound on e_u when the square nonlinearity in Figure 5 is included can be easily derived from the bound on e_M.

4.1 Inversion of the Preisach operator Γ

If the Preisach measure ν is given, and if it is nonnegative and nonsingular, an iterative inversion algorithm is available and $\| e_M \| \leq \epsilon$, where ϵ is the stopping criterion [17].

If ν is unknown, we can obtain a nonsingular approximation ν_p with a piecewise uniform density μ_p as discussed in Section 2. The Preisach operator with measure ν_p can be inverted exactly (in finite number of steps) [17]. Hence the inversion error e_M is solely due to the measure error $|\nu - \nu_p|$. It turns out that we can quantify the error bound in terms of the relative error of identification and the discretization level L of the Preisach plane:

Proposition 4.1 *Let the true Preisach measure ν be nonnegative and nonsingular with density μ. Let μ be bounded by a constant $\bar{\mu} > 0$. Given a discretization of level L, denote the integral of μ over a cell i as ν_i^0, $1 \le i \le N_c$, where N_c is the total number of cells. Denote by ν_i the identified mass for cell i. Assume the relative error in identification is δ_I, i.e., $\frac{|\nu_i - \nu_i^0|}{\nu_i^0} \le \delta_I,\ 1 \le i \le N_c$. Then*

$$\| e_M \|_\infty \le \delta_I M_s + \frac{8\bar{\mu} r_0^2}{L},$$

where M_s is the positive saturation corresponding to ν.

The proof is omitted due to space limitation and it can be found in [17].

4.2 Inversion of (5)

An inversion scheme was proposed for the model (5) [18]. But if there is uncertainty in the model parameters, it is very hard to derive a bound for the inversion error. We now present another inversion algorithm. Eq. (5) can be rewritten as:

$$\begin{cases} \dot{H}(t) = \frac{c_1}{1+g(t)}(I(t) - \frac{H(t)}{c_0}) \\ M(t) = \Gamma[H(\cdot), \psi_0](t) \end{cases}, \tag{6}$$

where $g(t)$ carries the interpretation of "$\frac{dM}{dH}$" at time t, and it depends on both the state ψ_t (the memory curve at t) and the sign of $\dot{H}$ [17]. Under mild conditions, $0 \le g(t) \le C$. We can view (6) as perturbed from the following decoupled system:

$$\begin{cases} \dot{H}(t) = \frac{c_1}{1+\bar{g}}(I(t) - \frac{H(t)}{c_0}) \\ M(t) = \Gamma[H(\cdot), \psi_0](t) \end{cases}, \tag{7}$$

where $\bar{g} \in [0, C]$ is some constant. Based on (7), an *approximate* inversion scheme for (6) is given formally by

$$\begin{cases} H(t) = \Gamma^{-1}[M(\cdot), \psi_0](t) \\ I(t) = \frac{1+\bar{g}}{c_1}\dot{H}(t) + \frac{H(t)}{c_0} \end{cases}. \tag{8}$$

In the discrete-time implementation, a delay is introduced in the inversion due to the dynamics. Hence the inversion error is defined as $e_M[k] \stackrel{\triangle}{=} \tilde{M}[k] - M[k-1]$. We can choose an explicit or implicit Euler scheme in discretizing (5) and (8), and for either scheme, we can quantify the error bound in terms of model parameters, see [17].

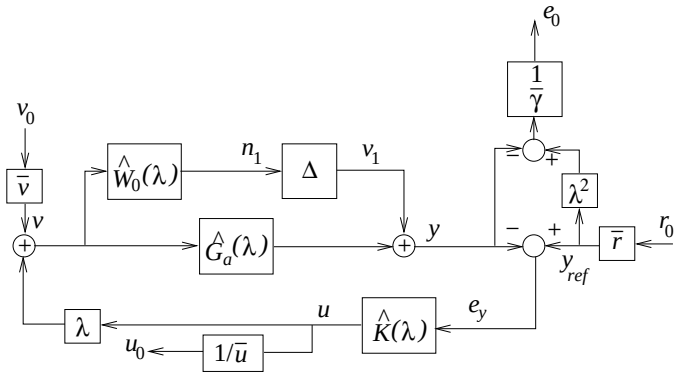

Figure 6: Robust control of a magnetostrictive actuator.

Remark 4.1 *The inversion algorithm (8) leads to an inversion error even if the exact parameters are known. But the payoff is that, this scheme allows us to quantify the inversion error when parameter errors are present.*

5 Formulation of the Robust Control Problem

In this paper, we consider $\hat{G}_0(\lambda)$ to be the identity operator, i.e., we are interested in trajectory tracking of the actuator head itself. Figure 6 shows the closed-loop system after the inverse compensation is done, where the exogenous noise v represents the inversion error. From the previous section, $\| v \|_\infty \leq \bar{v}$, and $\bar{v}$ is quantifiable in terms of inverse schemes and parametric uncertainties. The composition $\Delta \circ \hat{W}_0(\lambda)$ represents the deviation of the actual plant from the nominal plant $\hat{G}_a(\lambda)$. We assume that Δ can be any nonlinear operator with $\| \Delta \|_{l_\infty - ind} < 1$. $\hat{W}_0(\lambda)$ is a weighting function and it reflects that the model uncertainty is larger at a higher frequency.

Let $\| y_{ref} \|_\infty \leq \bar{r}$, where y_{ref} is the reference trajectory. The error $e_y \stackrel{\triangle}{=} y_{ref} - y$ is fed into the controller $\hat{K}(\lambda)$. The delay λ following $\hat{K}(\lambda)$ is due to inversion of the dynamic hysteresis model. Let the saturation limits of the actuator be $-\bar{u}$ and $\bar{u}$ respectively. Then the saturation constraint translates into $\| u_0 \|_\infty \leq 1$, where u_0 is as defined in Figure 6. The case $u_{min} \neq -u_{max}$ can be handled by defining $\bar{u} = \frac{u_{max} - u_{min}}{2}$ and $u_b = \frac{u_{max} + u_{min}}{2}$, where u_b is a bias input to be injected into the system [17].

There are two delays in the loop since $\hat{G}_a(\lambda)$ contains a pure delay. This motivates us to define the tracking error e_0 as

$$e_0[k] = \frac{y_{ref}[k-2] - y[k]}{\gamma}, \tag{9}$$

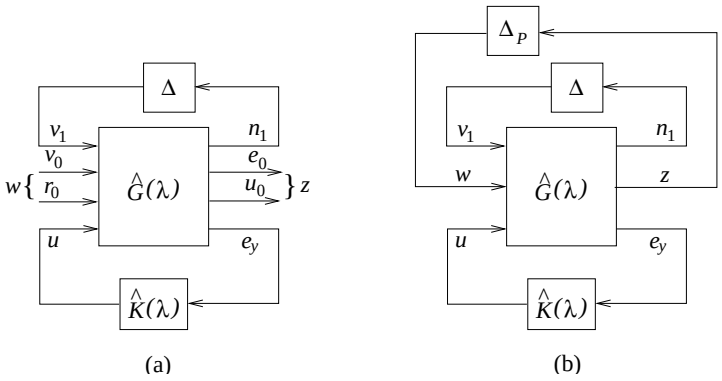

Figure 7: Formulation of the robust control problem.

where $\gamma > 0$ is the desired disturbance attenuation level. To ease the formulation, we normalize signals v and y_{ref}, and regard v_0 and r_0 as inputs to the system with $\| v_0 \|_\infty \leq 1$, $\| r_0 \|_\infty \leq 1$ (Figure 6).

The transfer function $\hat{G}(\lambda)$ from $(v_1, v_0, r_0, u)^T$ to $(n_1, e_0, u_0, e_y)^T$ can be easily written down. In terms of $\hat{G}$, the closed-loop system in Figure 6 can be simplified as in Figure 7 (a).

The control objective is: find the smallest γ and a stabilizing controller $\hat{K}(\lambda)$, such that

1. the closed-loop system is stable for any Δ with $\| \Delta \|_{l_\infty - ind} < 1$,
2. $\| e_0 \|_\infty \leq 1$ if $\Delta = 0$, $\forall v_0$, r_0 with $\| v_0 \|_\infty \leq 1$ and $\| r_0 \|_\infty \leq 1$, and
3. $\| u_0 \|_\infty \leq 1$ if $\Delta = 0$, $\forall v_0$, r_0 with $\| v_0 \|_\infty \leq 1$ and $\| r_0 \|_\infty \leq 1$.

If we define the exogenous input w and the regulated output z as

$$w \stackrel{\triangle}{=} \begin{pmatrix} v_0 \\ r_0 \end{pmatrix}, \quad z \stackrel{\triangle}{=} \begin{pmatrix} e_0 \\ u_0 \end{pmatrix},$$

then items 2 and 3 above are equivalent to $\| \Phi_{zw} \|_1 \leq 1$,, where Φ_{zw} denotes the transfer function from w to z, and $\| \cdot \|_1$ denotes the l_1 norm of a LTI system [2]. By the small gain theorem, (5) is equivalent to requiring robust stability of the system when we wrap a nonlinear uncertainty block Δ_P from z to w with $\| \Delta_P \|_{l_\infty - ind} < 1$, as shown in Figure 7 (b).

Now the control problem can be reformulated as: find the smallest γ and a stabilizing controller $\hat{K}(\lambda)$, such that the closed-loop system in Figure 7 (b) is robustly stable for all $\tilde{\Delta} \in \tilde{\mathbf{\Delta}}$, where $\tilde{\mathbf{\Delta}} \stackrel{\triangle}{=} \{\tilde{\Delta} = diag(\Delta, \Delta_P) : \Delta$ is nonlinear and of dimension 1×1, Δ_P is nonlinear and of dimension 2×2, $\| \tilde{\Delta} \|_{l_\infty - ind} < 1\}$.

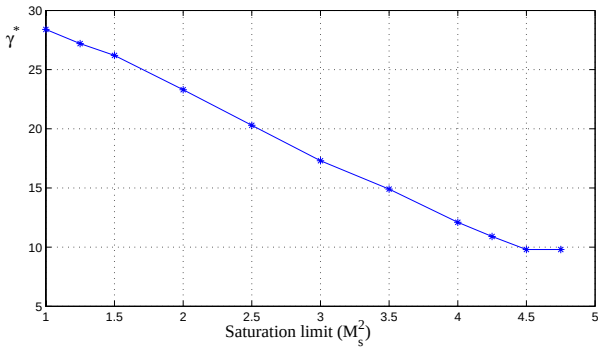

Figure 8: Effect of the saturation limit on γ^*.

To solve the robust control problem, we need determine, for a fixed $\gamma > 0$, whether we can find a stabilizing $\hat{K}(\lambda)$, such that the closed-loop system is stable for all $\tilde{\Delta} \in \tilde{\mathbf{\Delta}}$. This will be called *the robust control problem with disturbance attenuation level* γ, and it is solvable if and only if

$$\inf_{\text{stabilizing } \hat{K}} \inf_{D \in \mathbf{D}} \| D^{-1} F_l(\hat{G}, \hat{K}) D \|_1 \leq 1, \tag{10}$$

where $\mathbf{D} \stackrel{\triangle}{=} \{D = diag(d_1, d_2, d_2) : d_1, d_2 > 0\}$, and $F_l(\cdot, \cdot)$ denotes the lower Linear Fractional Transformation [2]. How to solve (10) can be found in [2] and is omitted here.

6 Simulation and Experimental Results

6.1 Effects of design parameters on γ^*

We first present computation results on how the optimal attenuation level γ^* is affected by the design parameters. Corresponding to the sampling frequency 2000 Hz, $\hat{G}_a(\lambda) = \frac{2.23\times10^{-11}\lambda^2+4.28\times10^{-11}\lambda}{0.147\lambda^2-0.549\lambda+1}$, and $\hat{W}_0(\lambda) = \frac{1.1759c_w(\lambda-1.0005)}{\lambda-1.1765}$, where $c_w > 0$ determines the magnitude of the uncertainty. We let $\bar{r} = 30$.

Figure 8 shows how γ^* is affected by the saturation constraint $\bar{u}$. We have used $c_w = 6.53 \times 10^{-13}$ and $\bar{v} = 0.1M_s^2$, where M_s is the saturation magnetization. Since the range of u for the magnetostrictive actuator is $[0, M_s^2]$, expressing $\bar{v}$ and $\bar{u}$ in terms of M_s^2 allows one to make more concrete sense out of these numbers. From Figure 8, γ^* drops when $\bar{u}$ increases, but γ^* becomes a constant when $\bar{u}$ hits $4.5M_s^2$, beyond which the saturation constraint no longer plays a role. Effects of c_w and $\bar{v}$ on γ^* have also been studied, and we find that γ^* drops as c_w or $\bar{v}$ does so [17].

6.2 Results of trajectory tracking

As we have seen from Figure 8, the tracking performance deteriorates as the saturation constraint $\bar{u}$ is tightened. For the magnetostrictive actuator, $\bar{u} = 0.5M_s^2$ and strictly enforcing this constraint will lead to large tracking errors. This reveals the limitation of pure linear design for an intrinsically nonlinear plant. Hence a practical approach would be properly relaxing the constraint.

Figure 9(a) shows the simulation result of tracking a sinusoidal signal. The current I applied is also displayed. The controller $\hat{K}(\lambda)$ is designed based on $c_w = 3.3 \times 10^{-13}$, $\bar{v} = 0.1M_s^2$, and $\bar{u} = 3.25M_s^2$. Figure 10 shows the output of $\hat{K}(\lambda)$, and we see that although we set $\bar{u} = 3.25M_s^2$ in the controller design, the control stays in the (true) unsaturated region $[-0.5M_s^2, 0.5M_s^2]$ except during the transient period at the beginning.

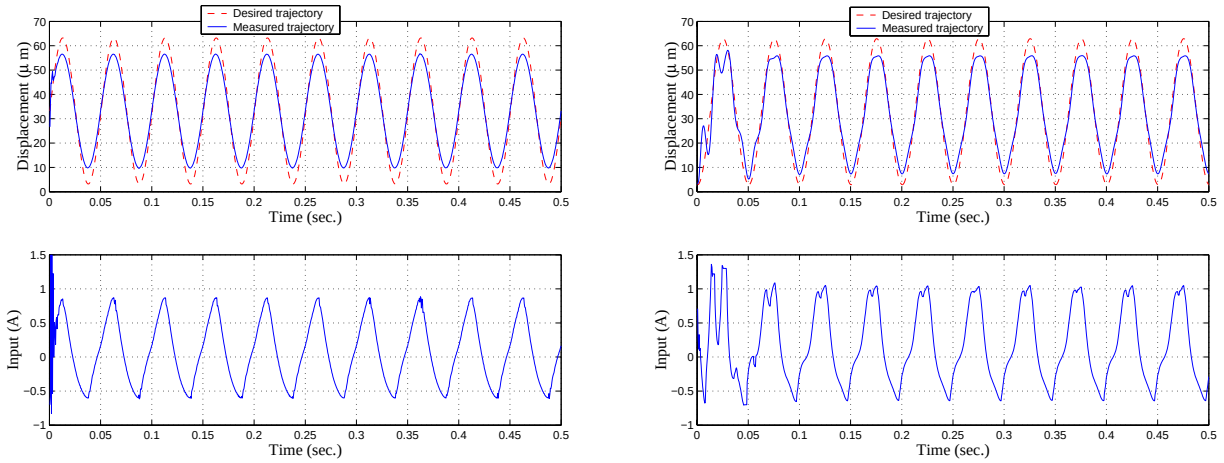

(a) (b)

Figure 9: (a) Simulation result of trajectory tracking; (b) Experimental result of trajectory tracking.

Our composite controller (the linear robust controller plus the inverse algorithm) is compuation

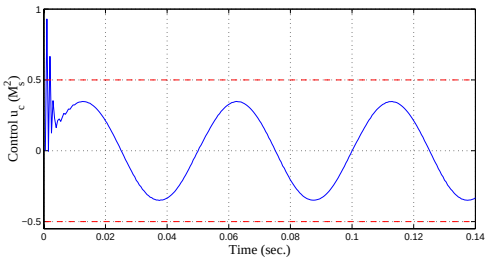

Figure 10: The control output u_0.

efficient and we can implement it in real-time. Figures 9(b) shows the experimental result of trajectory tracking based on the same controller used in the simulation. It matches well with the simulation result and the overall performance is satisfactory. We have also performed simulation and experiment of tracking an irregular signal, and the results are similar to those in Figures 9(a) and 9(b) [17].

The saturation limit $\bar{u}$ can not be "over-relaxed". For example, we design another controller based on $\bar{r} = 25$, $c_w = 3.3 \times 10^{-13}$, $\bar{v} = 0.05 M_s^2$, and $\bar{u} = 5 M_s^2$. The simulation result (Figures 11(a)) based on this new controller is better than that in Figure 9(a). But when we put the controller into the experiment, the tracking performance suffers from the persistant saturation (Figure 11(b)).

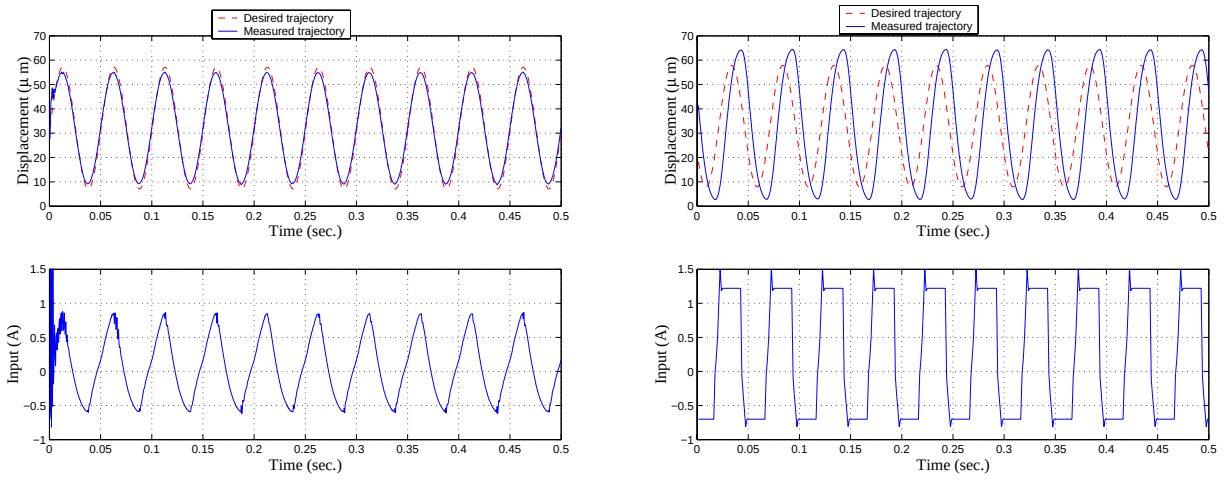

(a) (b)

Figure 11: Results based on an "over-relaxed" controller. (a) Simulation result of trajectory tracking; (b) Experimental result of trajectory tracking.

7 Conclusions

In this paper, we have presented a robust control framework for smart actuators by combining the inverse compensation with the linear robust control theory. We studied inversion schemes for the Preisach operator-based hysteretic models and modeled the inversion error as an exogenous noise whose magnitude bound is quantifiable. Robust control techniques were then employed to attenuate the impact of the inversion error as well as ensure stability in the presence of uncertainty. The saturation constraint was also incorporated into the controller design. Simulation and experimental results have demonstrated the

effectiveness of the approach.

8 Acknowledgement

The authors would like to acknowledge useful discussions with Professors R. Venkataraman, P. S. Krishnaprasad, and A. Tits.

References

[1] R. Venkataraman and P. S. Krishnaprasad, "Approximate inversion of hysteresis: theory and numerical results," in *Proceedings of the 39th IEEE Conference on Decision and Control*, Sydney, Australia, Dec. 2000, pp. 4448–4454.

[2] M. A. Dahleh and I. J. Diaz-Bobillo, *Control of Uncertain Systems: A Linear Programming Approach*, Prentice-Hall, Englewood Cliffs, NJ, 1995.

[3] D. Hughes and J. T. Wen, "Preisach modeling and compensation for smart material hysteresis," in *Active Materials and Smart Structures*, G. L. Anderson and D. C. Lagoudas, Eds., 1994, vol. 2427 of *SPIE*, pp. 50–64.

[4] G. Tao and P. V. Kokotović, "Adaptive control of plants with unknown hysteresis," *IEEE Transactions on Automatic Control*, vol. 40, no. 2, pp. 200–212, 1995.

[5] R. C. Smith, "Inverse compensation for hysteresis in magnetostrictive transducers," Tech. Rep. CRSC-TR98-36, CRSC, North Carolina State University, 1998.

[6] W. S. Galinaitis and R. C. Rogers, "Control of a hysteretic actuator using inverse hysteresis compensation," in *Mathematics and Control in Smart Structures*, V.V. Varadan, Ed., 1998, vol. 3323 of *SPIE*, pp. 267–277.

[7] X. Tan, R. Venkataraman, and P. S. Krishnaprasad, "Control of hysteresis: Theory and experimental results," in *Modeling, Signal Processing, and Control in Smart Structures*, V. S. Rao, Ed., 2001, vol. 4326 of *SPIE*, pp. 101–112.

[8] P. Ge and M. Jouaneh, "Tracking control of a piezoceramic actuator," *IEEE Transactions on Control Systems Technology*, vol. 4, no. 3, pp. 209–216, 1996.

[9] R. B. Gorbet, D. W. L. Wang, and K. A. Morris, "Preisach model identification of a two-wire SMA actuator," in *Proceedings of IEEE International Conference on Robotics and Automation*, 1998, pp. 2161–2167.

[10] I. D. Mayergoyz, *Mathematical Models of Hysteresis*, Springer Verlag, 1991.

[11] A. Visintin, *Differential Models of Hysteresis*, Springer, 1994.

[12] M. Brokate and J. Sprekels, *Hysteresis and Phase Transitions*, Springer Verlag, New York, 1996.

[13] G. Tao and P. V. Kokotović, *Adaptive Control of Systems with Actuator and Sensor Nonlinearities*, John Wiley & Sons, Inc, 1996.

[14] H. L. Royden, *Real Analysis*, Prentice Hall, Englewood Cliffs, NJ, 1988.

[15] R. Venkataraman, *Modeling and Adaptive Control of Magnetostrictive Actuators*, Ph.D. thesis, University of Maryland, College Park, 1999.

[16] R. Venkataraman and P. S. Krishnaprasad, "A model for a thin magnetostrictive actuator," in *Proceedings of the 32nd Conference on Information Sciences and Systems, Princeton, NJ*, Princeton, Mar. 1998.

[17] X. Tan, *Control of Smart Actuators*, Ph.D. thesis, University of Maryland, College Park, MD, Sept. 2002, available online at http://www.isr.umd.edu/TechReports/ISR/2002, in the PhD Thesis section.

[18] X. Tan and J. S. Baras, "Modeling and control of a magnetostrictive actuator," in *the Proceedings of the 41st IEEE Conference on Decision and Control (to appear)*, Las Vegas, NV, 2002.